Phenomenological Description of the Two Energy Scales in Underdoped Cuprate Superconductors

B. Valenzuela* and E. Bascones†

Instituto de Ciencia de Materiales de Madrid, CSIC, Cantoblanco, E-28049 Madrid, Spain

(Received 8 November 2006; published 29 May 2007)

Raman and angle-resolved photoemission spectroscopy experiments have demonstrated that in superconducting underdoped cuprates nodal and antinodal regions are characterized by two energy scales instead of the one expected in BCS theory. The nodal scale decreases with underdoping while the antinodal one increases. Contrary to the behavior expected for an increasing energy scale, the antinodal Raman intensity decreases with decreasing doping. Using the Yang-Rice-Zhang model, we show that these features are a consequence of the nonconventional nature of the superconducting state in which superconductivity and pseudogap correlations are both present and compete for the phase space.

DOI: 10.1103/PhysRevLett.98.227002 PACS numbers: 74.72.−h, 71.10.−w, 78.20.Bh

The pseudogap (PG) state of underdoped (UD) cuprates is characterized by a nodal-antinodal dichotomy with Fermi arcs at the diagonals of the Brillouin zone (BZ) (nodal region) and a gapped antinodal region [1,2]. Raman [3,4] and angle-resolved photoemission (ARPES) experiments [5] have confirmed that a nodal-antinodal dichotomy is also present in the superconducting (SC) state [6] which suggests that the SC state cannot be simply described by BCS theory, contrary to general belief [7].

Inelastic Raman scattering probes the zero-momentum charge excitations. The response of nodal ($\chi_{B_{2g}}$) and antinodal regions ($\chi_{B_{1g}}$) can be separated. In the SC state pair-breaking peaks appear in the spectra. As the normal state of cuprates is characterized by a not yet understood broad continuum, these peaks are better identified in the subtracted response in SC and normal states $\Delta\chi_{B_{1g,2g}} = \chi^{\mathrm{SC}}_{B_{1g,2g}} - \chi^{N}_{B_{1g,2g}}$. In a standard d-wave BCS gap $\Delta_S \cos(2\phi)$, the frequency and intensity of both B_{2g} and B_{1g} peaks are only controlled by Δ_S.

The experiments [3] reveal that in UD cuprates $\Delta\chi_{B_{1g}}$ and $\Delta\chi_{B_{2g}}$ show pair-breaking peaks with opposite evolution with doping, instead of the single-energy scale Δ_S. The B_{1g} peak shifts to higher energy and loses intensity with underdoping, while the B_{2g} peak shifts to lower frequency without too much change in intensity. The Raman B_{1g} response has been one of the experimental results that is more difficult to understand. A modified BCS gap with higher harmonics [3], and vertex corrections [8] or a strong anisotropic renormalization of the quasiparticle [3], have been invoked to explain the B_{1g} spectrum.

ARPES measurements [5] also uncovered that underdoping increases the gap in the antinodal region $\Delta_{\max}$ and decreases the slope of the gap at the nodes, v_Δ, resulting in a U-shaped dependence of the gap [5]. A single-energy scale and a V-shaped gap linear in $\cos(2\phi)$ are seen in ARPES (and Raman) in overdoped cuprates [2,4].

In this Letter, we show that the appearance of nodal and antinodal energy scales and the suppression of intensity of $\Delta\chi_{B_{1g}}$ with underdoping are a consequence of the nonconventional nature of the SC state in which superconductivity and PG correlations are both present and compete for the phase space. We assume that the PG strength, given by Δ_R vanishes at a topological quantum critical point (QCP), and that the SC order parameter Δ_S follows the critical temperature. Figure 1 and the evolution of the Raman intensity with doping x are our main results. Only the nodal energy scales follow the nonmonotonic dependence of the SC order parameter; the slope of the gap at the nodes v_Δ is a good measure of Δ_S. The antinodal energy scale, i.e., the location of the B_{1g} Raman peak $\omega_{B_{1g}}$ and the maximum gap $\Delta_{\max}$ in ARPES, is intimately connected with the PG. The intensity decrease in B_{1g} with underdoping is not due to vertex corrections, but to the competition of PG and superconductivity in the antinodal region. The suppression of the quasiparticle weight just enhances it.

We use the ansatz proposed by Yang, Rice, and Zhang (YRZ) [9] for the PG. The YRZ model assumes that the PG

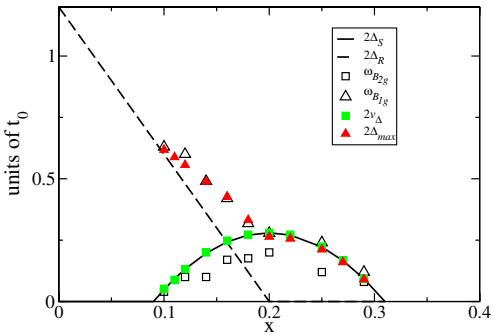

FIG. 1 (color online). Comparison of pseudogap Δ_R and superconducting Δ_S scales with ARPES nodal v_Δ and antinodal $\Delta_{\max}$ ones and with the frequency at which B_{1g} ($\omega_{B_{1g}}$) and B_{2g} ($\omega_{B_{2g}}$) Raman responses peak. The parameters used depend on doping as $\Delta_R(x)/2 = 0.3(1 - x/0.2)$, $\Delta_S(x)/2 = 0.07[1 - 82.6(x - 0.2)^2]$, $t(x) = g_t(x) + 0.169/(1 + x)^2$, $|t'(x)| = g_t(x)|t'_0|$ with $t'_0 = -0.3$, $t''(x) = g_t(x)t''_0$ with $t''_0 = 0.2$. All energies are in units of the bare hopping t_0.

can be described as a doped spin liquid and proposes a phenomenological Green's function to characterize it:

$$G^{\mathrm{YRZ}}(\mathbf{k},\omega)=\frac{g_t}{\omega-\xi_{\mathbf{k}}-\Sigma_R(\mathbf{k},\omega)}+G_{inc}. \quad (1)$$

Here $\xi_{\mathbf{k}}=\epsilon_{0\mathbf{k}}-4t'(x)\cos k_x\cos k_y-2t''(x)(\cos 2k_x+\cos 2k_y)-\mu_p$, $\epsilon_{0\mathbf{k}}=-2t(x)(\cos k_x+\cos k_y)$, and μ_p is determined from the Luttinger sum rule. $\Sigma_R(\mathbf{k},\omega)=\Delta_R(\mathbf{k})^2/(\omega+\epsilon_{0\mathbf{k}})$ diverges at zero frequency at the umklapp surface $\epsilon_{0\mathbf{k}}$, and $\Delta_R(\mathbf{k})=\Delta_R(x)/2(\cos k_x-\cos k_y)$. The coherent part is similar to the BCS diagonal Green's function with the nontrivial difference that in BCS the self-energy diverges at the Fermi surface (FS) and not at the umklapp one. Besides there is no off-diagonal component of the Green's function in our case and Δ_R does not break any symmetry. For finite Δ_R the quasiparticle peak is split into two and the FS consists of hole pockets close to $(\pm\pi/2,\pm\pi/2)$. At x_c, $\Delta_R(x)$ vanishes at a topological transition and a complete FS is recovered. The coherent spectral weight, $g_t=2x/(1+x)$, decreases with underdoping and vanishes at half filling [10]. We use the same parameters as in the original paper [9]; see Fig. 1.

Superconductivity is introduced in the standard way [11], as in Ref. [9], through a SC self-energy $\Sigma_S(\mathbf{k},\omega)=|\Delta_S^2(\mathbf{k})|/(\omega+\xi(\mathbf{k})+\Sigma_R(\mathbf{k},-\omega))$ where $\Delta_S(\mathbf{k})=\Delta_S(x)/2(\cos k_x-\cos k_y)$. Each quasiparticle peak splits into four with energies $\pm E_\pm$:

$$(E_{\mathbf{k}}^{\pm})^2=\Delta_{R\mathbf{k}}^2+\frac{\xi_{\mathbf{k}}^2+\xi_{0\mathbf{k}}^2+\Delta_{S\mathbf{k}}^2}{2}\pm(E_{\mathbf{k}}^{\mathrm{SC}})^2,$$

$$(E_{\mathbf{k}}^{\mathrm{SC}})^2=\sqrt{(\xi_{\mathbf{k}}^2-\xi_{0\mathbf{k}}^2+\Delta_{S\mathbf{k}}^2)^2+4\Delta_{R\mathbf{k}}^2((\xi_{\mathbf{k}}-\xi_{0\mathbf{k}})^2+\Delta_{S\mathbf{k}}^2)}.$$

The spectral functions $A(\mathbf{k},\omega)=-2\mathrm{Im}G(\mathbf{k},\omega)$ and $B(\mathbf{k},\omega)=-2\mathrm{Im}F(\mathbf{k},\omega)$ with $F(\mathbf{k},\omega)$ the anomalous Green's function are

$$\begin{aligned}A(\mathbf{k},\omega)&=g_t\pi\{(v_{\mathbf{k}}^-)^2\delta(\omega+E_{\mathbf{k}}^-)+(u_{\mathbf{k}}^-)^2\delta(\omega-E_{\mathbf{k}}^-)\\&\quad+(v_{\mathbf{k}}^+)^2\delta(\omega+E_{\mathbf{k}}^+)+(u_{\mathbf{k}}^+)^2\delta(\omega-E_{\mathbf{k}}^+)\},\\B(\mathbf{k},\omega)&=g_t\pi\{u_{\mathbf{k}}^-v_{\mathbf{k}}^-[\delta(\omega+E_{\mathbf{k}}^-)+\delta(\omega-E_{\mathbf{k}}^-)]\\&\quad+u_{\mathbf{k}}^+v_{\mathbf{k}}^+[\delta(\omega+E_{\mathbf{k}}^+)+\delta(\omega-E_{\mathbf{k}}^+)]\},\end{aligned} \quad (2)$$

with coherence factors $v_{\mathbf{k}}^{2\pm}=\frac{1}{2}(a_{\mathbf{k}}^{\pm}-b_{\mathbf{k}}^{\pm}/E_{\mathbf{k}}^{\pm})$ and $u_{\mathbf{k}}^{2\pm}=\frac{1}{2}(a_{\mathbf{k}}^{\pm}+b_{\mathbf{k}}^{\pm}/E_{\mathbf{k}}^{\pm})$, where $a_{\mathbf{k}}^{\pm}=\frac{1}{2}[1\pm(\xi_{\mathbf{k}}^2-\xi_{\mathbf{k0}}^2+\Delta_{S\mathbf{k}}^2)/E_{\mathbf{k}}^{\mathrm{SC}}]$ and $b_{\mathbf{k}}^{\pm}=\xi_{\mathbf{k}}a_{\mathbf{k}}^{\pm}\pm\Delta_{R\mathbf{k}}^2(\xi_{\mathbf{k}}-\xi_{\mathbf{k0}})$.

In the bubble approximation [12] the Raman response is

$$\begin{aligned}\mathrm{Im}\{\chi_{\gamma_\nu}(\Omega)\}&=\sum_{\mathbf{k}}(\gamma_{\mathbf{k}}^{\nu})^2\int\frac{d\omega}{4\pi}[n_F(\omega)-n_F(\omega+\Omega)]\\&\quad\times\{A(\mathbf{k},\omega+\Omega)A(\mathbf{k},\omega)\\&\quad-B(\mathbf{k},\omega+\Omega)B(\mathbf{k},\omega)\}.\end{aligned} \quad (3)$$

Here $n_F(\omega)$ is the Fermi function, $\nu=B_{1g}$, B_{2g}, and $\gamma_{\mathbf{k}}^{\nu}$, the B_{1g} and B_{2g} Raman vertices, are proportional to $\cos k_x-\cos k_y$ and $\sin k_x\sin k_y$, respectively.

The x dependence of the nodal and antinodal subtracted Raman spectra $\Delta\chi$ can be seen in Figs. 2(a) and 2(b). Two different energy scales $\omega_{B_{1g}}$ and $\omega_{B_{2g}}$ appear for finite Δ_R. These scales, signaled in Fig. 2, are plotted in Fig. 1. At $x_c=0.2$ the PG vanishes and $\Delta\chi_{B_{1g}}$ and $\Delta\chi_{B_{2g}}$ peak at an energy close to $2\Delta_S$, as expected in BCS [13]. On the contrary, as x is reduced the $\Delta\chi_{B_{1g}}$ peak shifts to larger frequency and its intensity decreases, while the $\Delta\chi_{B_{2g}}$ peak shifts to lower frequency with a weakly x-dependent intensity. This behavior resembles the experimental one [3]. In Figs. 2(a) and 2(b) the spectra have been divided by g_t^2 to emphasize that the suppression of the intensity in the B_{1g} channel with underdoping is not only due to the reduction of the coherent spectral weight, as proposed in [3]. With g_t^2 included, the weakening of the B_{1g} transition with underdoping is enhanced and the B_{2g} signal decreases.

The two different energy scales for B_{1g} and B_{2g} response are associated to the two pair-breaking transitions in the inset of Fig. 2(c) with energies $2E_\pm(\mathbf{k})$. The distinction between nodal and antinodal signal has its origin in the coherence factors $u_\pm^2(\mathbf{k})v_\pm^2(\mathbf{k})$ which weight each transition. Shown in Fig. 3(a) [Fig. 3(b)] for $x=0.14$, $u_-^2(\mathbf{k})v_-^2(\mathbf{k})$ ($u_+^2(\mathbf{k})v_+^2(\mathbf{k})$) weights more heavily the nodal (antinodal) region. The B_{2g} and B_{1g} spectra are, respectively, dominated by the transitions with energy $2E_-$ and $2E_+$. The maxima in the Raman spectra in Figs. 2(a) and 2(b) arise from the peaks in the densities of transitions $N_{2E_\pm}^{\mathrm{weight}}=\sum_{\mathbf{k}}u_\pm^2(\mathbf{k})v_\pm^2(\mathbf{k})\delta[\omega-2E_\pm(\mathbf{k})]$. In Fig. 3(d) $N_{2E_-}^{\mathrm{weight}}$ peaks at a frequency smaller than $2\Delta_S$. $\omega_{B_{2g}}$ de-

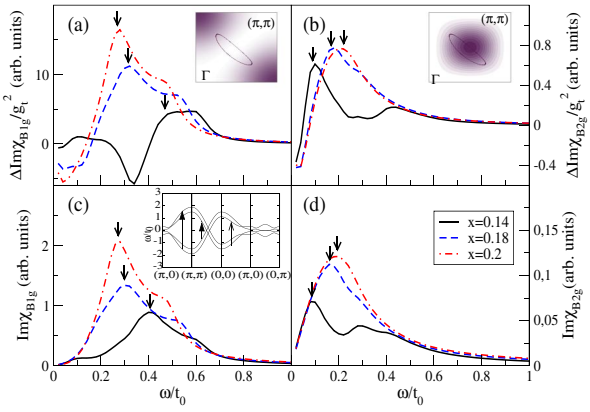

FIG. 2 (color online). Insets in (a) and (b): Raman vertices $(\gamma_{\mathbf{k}}^{B_{1g}})^2$ and $(\gamma_{\mathbf{k}}^{B_{2g}})^2$ in the first quadrant of the Brillouin zone, with the Fermi pocket for $x=0.14$. Inset in (c): Bands for $x=0.14$ in the SC state. The arrows signal the possible optical transitions. (a),(b) Subtracted Raman response in B_{1g} and B_{2g} channels divided by the coherent weight factor g_t^2, for $x=0.14$ and $x=0.18$ in the underdoped regime and to $x_c=0.20$. (c),(d) B_{1g} and B_{2g} full Raman spectrum for the same dopings. Units are the same for all dopings. The arrows indicate the position, $\omega_{B_{1g}}$ and $\omega_{B_{2g}}$, of the pair-breaking peaks. δ functions in Eq. (2) are replaced by Lorenzians of width $0.05t(x)$.

pends not only on Δ_S but also on the length of the Fermi pockets along $(\pi, 0)$-$(0, \pi)$ as its value comes from the edges of the Fermi pockets. Because of the shrinking of the pockets with increasing Δ_R, $\omega_{B_{2g}}$ is shifted to lower frequencies with underdoping, even if a doping independent Δ_S is used. In Fig. 3(e), the energy at which $N^{\text{weight}}_{2E_+}$ peaks is determined by a saddle point close to $(\pi, 0)$, along $(\pi, 0)$-(π, π) and is bigger than $2\Delta_S$. In the UD region, this energy is mainly controlled by Δ_R. If $x \geq x_c$, only one of the pair-breaking transitions contributes for a given $\mathbf{k}$. A complete d-wave SC gap is recovered and, as shown in Fig. 3(c), it is tracked by the added coherence factors $u^2_+(\mathbf{k})v^2_+(\mathbf{k}) + u^2_-(\mathbf{k})v^2_-(\mathbf{k})$. The maximum in $N^{\text{weight}}_{E_-}$ is no longer a maximum of the total density $N^{\text{weight}}_{\text{tot}} = N^{\text{weight}}_{E_-} + N^{\text{weight}}_{E_+}$, plotted in Fig. 3(f), but both densities of transitions match perfectly. $N^{\text{weight}}_{\text{tot}}$ is now the meaningful quantity. It peaks close to $2\Delta_S$ recovering the BCS single-energy behavior [13].

A third *crossing* transition, with energy $E_-(\mathbf{k}) + E_+(\mathbf{k})$, and larger intensity in the B_{1g} channel is also allowed if Δ_R is finite, as shown in the inset of Fig. 2(c). Its effect is small in $\Delta\chi$, as expected in both the PG and the SC state. The total responses $\chi^{\text{SC}}_{B_{1g}}$ and $\chi^{\text{SC}}_{B_{2g}}$ including the contribution of this crossing transition in the SC state are plotted in Figs. 2(c) and 2(d). It is not easy to distinguish this transition from the pair-breaking ones. To the best of our knowledge this transition has not been found yet in the PG state, but it could be hidden in the broad background.

As expected for a gap with nodes, the B_{2g} response in Fig. 2(d) is linear at low frequencies. The slope is doping independent. This independence, observed also experimentally [3], comes from a cancellation of the dependencies of the quasiparticle weight squared g_t^2, Δ_S, and the density of states, via the renormalization of the band.

The nodal and antinodal scales can also be seen in ARPES. Because of the weak spectral weight in the outer edge of the FS pocket, the ARPES spectra resembles the Fermi arcs observed experimentally [9]. The length of these arcs increases with x, as seen in Figs. 4(a) and 4(b). A complete FS is recovered when $\Delta_R = 0$ in Fig. 4(c). In the absence of a complete FS, to analyze the $\mathbf{k}$ dependence of the gap we take the surface with maximal intensity $\omega = 0$ and $\Delta_S = 0$. This surface, marked in the pictures, resembles the one interpreted experimentally as the underlying FS. To compare with experiments [5] we define v_Δ as the derivative of the energy with respect to $\cos k_x - \cos k_y$ at the nodes [14] and $\Delta_{\max}$ as the maximum gap along this surface. Shown in Fig. 4(d) for $x = 0.05$, when Δ_S is zero but Δ_R finite, the energy vanishes along the arc and a gap opens linearly with $\cos k_x - \cos k_y$ from the arc edge. $\Delta_{\max}$ increases with underdoping. A finite Δ_S opens a gap along the arc in Fig. 4(e). It depends linearly on $\cos k_x - \cos k_y$,

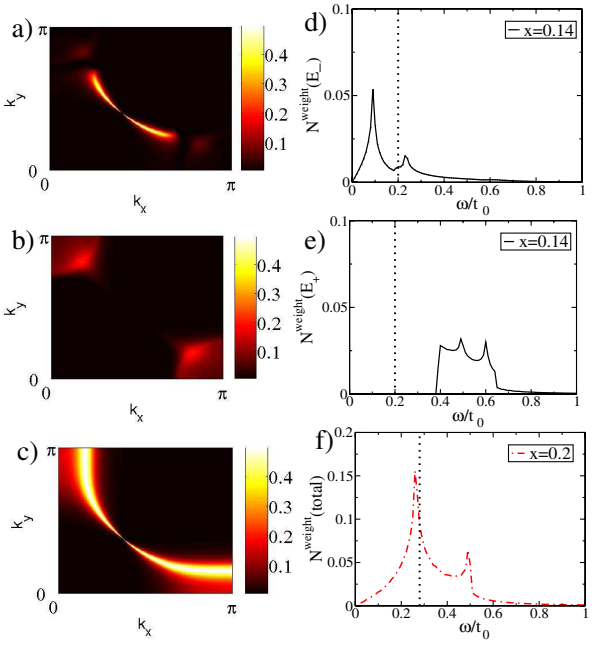

FIG. 3 (color online). (a)–(c) Coherence factors, in the first quadrant of the BZ, for the pair-breaking transitions with energies $2E_\pm$ (see text). (d)–(f) Weighted densities of transitions $N^{\text{weight}}(E_\pm)$. A dotted line marks $2\Delta_S$. The added coherence factors and total weighted density of transitions for $x_c = 0.2$ (critical doping) in (c) and (e) recover the BCS result.

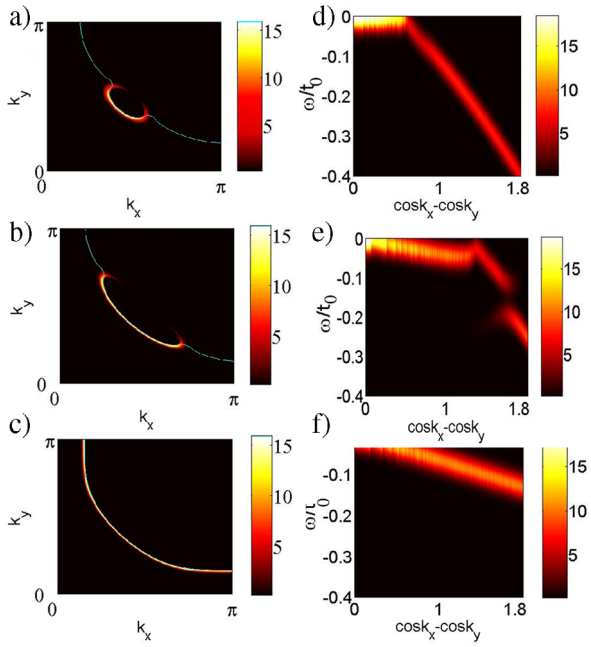

FIG. 4 (color online). (a)–(c) Map of ARPES in the first quadrant of the BZ, at zero frequency and zero Δ_S for (a) $x = 0.05$, (b) $x = 0.14$, and (c) $x_c = 0.20$. The light gray (blue) line corresponds to the maximum intensity surface. (d)–(f) Energy spectrum for (d) $x = 0.05$, (e) $x = 0.14$, and (f) $x = 0.20$, along the surface marked in (a)–(c). Δ_S is finite in (e) and (f). δ functions in $A(\mathbf{k}, \omega)$ are replaced by Lorenzians of width $0.001t_0$ and convoluted with a Gaussian of width $0.02t_0$ (~6–10 meV) and a temperature $T = 0.001t_0$.

with slope v_Δ very close to Δ_S. Outside the arc [15], the gap depends on both Δ_R and Δ_S. In this UD SC region v_Δ increases with x and $\Delta_{\max}$ decreases (see Fig. 1). Correspondingly, the spectra does not depend linearly on $\cos k_x - \cos k_y$ but has a U-shaped dependence on $\cos k_x - \cos k_y$ with a kink around the arc edge. Deviations increase with underdoping. In Fig. 4(f), at $x = x_c$, the linear V-shaped BCS dependence reappears and v_Δ and $\Delta_{\max}$ converge.

The evolution of ARPES scales v_Δ and $\Delta_{\max}$ with doping is plotted in Fig. 1, and compared with the ones found in Raman and the input Δ_S and Δ_R. The similarity with experimental data is striking [3]. With the $\Delta_S(x)$ used, $\omega_{B_{2g}}$ and v_Δ are nonmonotonic on doping. On the other hand, the frequency at which B_{1g} peaks $\omega_{B_{1g}}$ follows very closely $2\Delta_{\max}$ and both decrease as Δ_R does. Twice the gap value at $(\pi, 0)$, sometimes compared with $\omega_{B_{1g}}$, is expected to be larger than $2\Delta_{\max}$. The nodal and antinodal scales merge when the pseudogap correlations disappear.

In conclusion, we have reproduced the deviations from BCS in Raman and ARPES experiments in UD SC cuprates. Nodal and antinodal energy scales with opposite doping dependence appear in both spectra. The nodal B_{2g} response peaks at a frequency $\omega_{B_{2g}}$, which qualitatively follows the doping dependence of the SC order parameter Δ_S. On the contrary, the energy of the pair-breaking transitions in the antinodal region $\omega_{B_{1g}}$ decreases monotonically with increasing doping, and its intensity decreases with underdoping due to the competition between PG and SC correlations. Twice the maximum value of the ARPES antinodal gap follows very closely $\omega_{B_{1g}}$. Within this model the slope of the gap at the nodes, v_Δ, as measured by ARPES, is a good measure of Δ_S, while the maximum value of the gap $\Delta_{\max}$ arises from an interplay between the PG and Δ_S. We have not tried to fit the experiments but just taken the input values from YRZ [9].

Similar two-scale behavior could appear in other models with a QCP [16]. Possible differences could be the decreasing spectral weight with underdoping, important for the constancy of the slope in B_{2g} channel which *a priori* is not expected in other QCP models. In the YRZ ansatz the FS is truncated without breaking of symmetry and a topological transition happens at x_c, in agreement with experiments [17] and dynamical mean field theory [18]. Our results suggest that the PG is not a precursor to the superconductivity but has a different origin and persists in the SC state and that the antinodal scale depends on both the SC order parameter and the PG. The smooth convergence of the antinodal scale with the SC order parameter and a peak in $\Delta\chi_{B_{1g}}$ are hard to understand in models with separation in $\mathbf{k}$ space in which antinodal quasiparticles, responsible for the PG, do not participate in superconductivity [19]. While not included here, we believe that the two energy scales in the SC state are robust enough to survive inelastic scattering.

We thank M. Le Tacon, A. Sacuto, L. Tassini, R. Hackl, J. Carbotte, and G. Kotliar for discussions and M. A. H. Vozmediano, A. V. Chubukov, F. Guinea, and T. M. Rice for discussions and reading of the manuscript. Funding from MCyT through Grants No. MAT2002-0495-C02-01 and No. FIS2005-05478-C02-01 and Ramon y Cajal contract, CAM and CSIC through Grant No. 200550M136, and I3P contract is acknowledged.

*Electronic address: belenv@icmm.csic.es
†Electronic address: leni@icmm.csic.es

[1] T. Timusk and B. W. Statt, Rep. Prog. Phys. **62**, 61 (1999); M. R. Norman, D. Pines, and C. Kallin, Adv. Phys. **54**, 715 (2005).
[2] A. Damascelli, Z. Hussain, and Z.-X. Shen, Rev. Mod. Phys. **75**, 473 (2003).
[3] M. Le Tacon *et al.*, Nature Phys. **2**, 537 (2006).
[4] T. P. Devereaux and R. Hackl, Rev. Mod. Phys. **79**, 175 (2007).
[5] J. Mesot *et al.*, Phys. Rev. Lett. **83**, 840 (1999); S. V. Borisenko *et al.*, Phys. Rev. B **66**, 140509 (2002); Tanaka *et al.*, Science **314**, 1910 (2006); Kondo *et al.*, arXiv:cond-mat/0611517.
[6] C. Panagopoulos and T. Xiang, Phys. Rev. Lett. **81**, 2336 (1998).
[7] J. Zaanen *et al.*, Nature Phys. **2**, 138 (2006).
[8] R. Zeyher and A. Greco, Phys. Rev. Lett. **89**, 177004 (2002); Y. Gallais *et al.*, Phys. Rev. B **71**, 012506 (2005); A. V. Chubukov, T. P. Devereaux, and M. V. Klein, Phys. Rev. B **73**, 094512 (2006).
[9] K.-Y. Yang, T. M. Rice, and F.-C. Zhang, Phys. Rev. B **73**, 174501 (2006).
[10] F. C. Zhang, C. Gros, T. M. Rice, and H. Shiba, Supercond. Sci. Technol. **1**, 36 (1988).
[11] A. A. Abrikosov, L. P. Gor'kov, and I. E. Dzyaloshinaskii, in *Methods of Quantum Field Theory in Statistical Physics*, edited by R. A. Silverman (Dover, New York, 1975), revised ed.
[12] G. Mahan, *Many Particle Physics* (Plenum, New York, 1990).
[13] In the continuum the peak in $\Delta\chi_{B_{1g}}$ is at $2\Delta_S$. In a lattice two peaks appear, the one at higher energy is due to band structure effects and ignored in the discussion.
[14] v_Δ is normalized to $\Delta_{\max}$ for $\Delta(\phi) = \Delta_{\max}\cos(2\phi)$ [5].
[15] The suppression of the intensity for some $\mathbf{k}$ in the SC state is due to the mixing between the $\pm E_\pm$ bands.
[16] S. Chakravarty, R. B. Laughlin, D. K. Morr, and C. Nayak, Phys. Rev. B **63**, 094503 (2001); C. M. Varma, Phys. Rev. Lett. **83**, 3538 (1999); L. Benfatto, S. Caprara, and C. Di Castro, Eur. Phys. J. B **17**, 95 (2000).
[17] J. L. Tallon and J. W. Loram, Physica (Amsterdam) **349C**, 53 (2001).
[18] T. D. Stanescu and G. Kotliar, Phys. Rev. B **74**, 125110 (2006).
[19] D. Pines, arXiv:cond-mat/0404151.